



Carmichael, M. J., Pancost, R. D., & Lunt, D. J. (2018). Changes in the occurrence of extreme precipitation events at the Paleocene–Eocene thermal maximum. *Earth and Planetary Science Letters*, 501, 24-36. <https://doi.org/10.1016/j.epsl.2018.08.005>

Publisher's PDF, also known as Version of record

License (if available):
CC BY

Link to published version (if available):
[10.1016/j.epsl.2018.08.005](https://doi.org/10.1016/j.epsl.2018.08.005)

[Link to publication record in Explore Bristol Research](#)
PDF-document

This is the final published version of the article (version of record). It first appeared online via Elsevier at <https://www.sciencedirect.com/science/article/pii/S0012821X18304643> . Please refer to any applicable terms of use of the publisher.

University of Bristol - Explore Bristol Research

General rights

This document is made available in accordance with publisher policies. Please cite only the published version using the reference above. Full terms of use are available:
<http://www.bristol.ac.uk/red/research-policy/pure/user-guides/ebr-terms/>



Changes in the occurrence of extreme precipitation events at the Paleocene–Eocene thermal maximum

Matthew J. Carmichael^{a,b,c,*}, Richard D. Pancost^{b,c}, Daniel J. Lunt^{a,c}

^a BRIDGE, School of Geographical Sciences, University of Bristol, UK

^b Organic Geochemistry Unit, School of Chemistry and School of Earth Sciences, University of Bristol, UK

^c The Cabot Institute for the Environment, University of Bristol, UK

ARTICLE INFO

Article history:

Received 11 November 2017

Received in revised form 25 July 2018

Accepted 3 August 2018

Available online xxxx

Editor: M. Frank

Keywords:

extreme precipitation

proxy-model comparisons

General Circulation Model

Eocene

PETM

paleoclimate

ABSTRACT

Future global warming is widely anticipated to increase the occurrence of extreme precipitation events, but such hydrological changes have received limited attention within paleoclimate studies. Several proxy studies of the hydrological response to the Paleocene–Eocene Thermal Maximum hyperthermal, ~56 Ma, have recently invoked changes in the occurrence of extreme precipitation events to explain observations, but these changes have not been studied for the geologic past using climate models. Here, we use a coupled atmosphere–ocean general circulation model, HadCM3L, to study regional changes in metrics for extreme precipitation across the onset of the PETM by comparing simulations performed with possible PETM and pre-PETM greenhouse gas forcings. Our simulations show a shift in the frequency–intensity relationship of precipitation, with extreme events increasing in importance over tropical regions including equatorial Africa and southern America. The incidence of some extreme events increases by up to 70% across the PETM in some regions. While the most extreme precipitation rates tend to relate to increases in convective precipitation, in some regions dynamic changes in atmospheric circulation are also of importance. Although shortcomings in the ability of general circulation models to represent the daily cycle of precipitation and the full range of extreme events precludes a direct comparison of absolute precipitation rates, our simulations provide a useful spatial framework for interpreting hydrological proxies from this time period. Our results indicate that changes in extreme precipitation behaviour may be decoupled from those in mean annual precipitation, including, for example in east Africa, where the change in mean annual precipitation is small but a large increase in the size and frequency of extreme events occurs. This has important implications for the interpretation of the hydrological proxy record and our understanding of climatic, as well as biogeochemical, responses to global warming events.

© 2018 The Author(s). Published by Elsevier B.V. This is an open access article under the CC BY license (<http://creativecommons.org/licenses/by/4.0/>).

1. Introduction

Projections of how Earth's hydrological cycle will operate on a future warmer Earth indicate changes to the sub-annual character of precipitation including the frequency and intensity of extreme events (Emori and Brown, 2005; O'Gorman, 2015). Observational data indicate that in some mid-latitude regions, there has already been a disproportionate increase in heavy precipitation events relative to mean annual changes (Donat et al., 2013; Dittus et al., 2015). Changes in the occurrence of extreme precipitation are expected from thermodynamical effects of warming which increases the saturation vapour pressure of the atmosphere on the order of 7% K⁻¹, according to the Clausius–Clapeyron rela-

tion. In regions that are not moisture limited, there is subsequently an exponential increase in precipitable water, assuming that relative humidity remains constant. While the global precipitation rate is energetically constrained to ~2% K⁻¹ (Allen and Ingram, 2002), extreme events are predicted to scale with Clausius–Clapeyron, occurring where most atmospheric moisture is converted to precipitation (Dai and Trenberth, 2004). However, regional variations in the occurrence of extremes are more uncertain: dynamical changes in atmospheric circulation can lead to variations in moisture convergence, and observational studies have shown increases in extremes which exceed Clausius–Clapeyron scaling (Lenderink and van Meijgaard, 2008).

The instrumental record provides only a limited constraint on the behaviour of extreme precipitation in a warm world (e.g. Asadieh and Krakauer, 2015). As such, the response of the hydrological cycle to intervals of global warmth in the geologic record is receiving increased attention in paleoclimate studies (e.g. Pierrehumbert, 2002; Speelman et al., 2010). The environmental

* Corresponding author at: BRIDGE, School of Geographical Sciences, University of Bristol, UK.

E-mail address: Matt.Carmichael@bristol.ac.uk (M.J. Carmichael).

impacts of the Paleocene–Eocene Thermal Maximum (PETM) hyperthermal at ~56 Ma have received particular attention given the global nature of the 5–9 °C warming, and the event's rapid onset and transient nature (e.g. Dunkley-Jones et al., 2013). A range of proxies indicate that the warming was accompanied by a major hydrological perturbation, with evidence for increased continental runoff (John et al., 2008), excursions in oxygen and deuterium isotopes indicative of changes in precipitation amount and air mass history (Pagani et al., 2006) and changes in paleosol characteristics suggestive of variations in soil moisture (Kraus and Riggins, 2007).

Changes in the occurrence of hydrological extremes have previously been invoked to explain the results of a number of PETM proxy studies. In the Spanish Pyrenees, paleosol properties such as colouration, calcite content and presence of soil nodules indicate a semi-arid early Eocene climate with little soil moisture. Despite this, a 1–4 m thick conglomerate with clasts >65 cm marks the onset of the PETM (Schmitz and Pujalte, 2007) and is correlated with elevated coarse-grained sediment export elsewhere within the same basin (Pujalte et al., 2015). These changes have been interpreted as a response to the onset of high-energy storms with analogues drawn to modern-day megafans which form in regions with highly seasonal precipitation. Low-latitude PETM sections are scarce, but the Tanzanian Drilling Project (TDP) has provided indirect evidence for a change in subtropical precipitation regimes. Leaf wax biomarkers are isotopically enriched in deuterium at the PETM, which has been interpreted to reflect elevated evaporative enrichment in a more arid (i.e. reduced P–E) climate (Handley et al., 2012). However, these coincide with an increase in terrestrially-sourced biomarkers and elevated sedimentation rate, which led the authors to suggest that the region experienced increases in intense episodic, perhaps seasonal, precipitation events. Finally, at East Tasman Plateau (IODP Site 1172), the PETM is associated with a peak in the dinoflagellate *Eocladopyxis*. Based on studies of extant *Goniadomidae* – the family to which *Eocladopyxis* belongs – it has been suggested that the region experienced more storms at the PETM, at least seasonally, since in many regions this seems to be a requirement to re-suspend dormant cysts prior to their hatching (Sluijs et al., 2011 and references therein).

Reconstructing spatial changes in the characteristics of precipitation regimes at the PETM is a relatively new endeavour and is compounded by a scarcity of sections from low latitudes and terrestrial settings (e.g. Handley et al., 2012; Kraus et al., 2013). While thermodynamics suggests an increase in intense precipitation events should be expected during a global warming event such as the PETM, it is currently unknown whether particular regions were more susceptible than others to extremes. Furthermore, the existing evidence for extreme PETM precipitation comes from different proxies and spans a range of latitudes and environmental settings, such that it is unclear whether other regions also experienced changes in intense, episodic rainfall, or whether existing proxies for hydrological change at some locations have been erroneously interpreted as mean annual climatic signals. For example, several proxies for PETM hydrological changes relate to continental weathering and erosion (such as increased sedimentation rate, kaolinite deposition and geomorphological evolution, e.g. John et al., 2008; Foreman et al., 2012) or increased nutrient delivery to continental margins (Sluijs et al., 2014). Such proxies may incorporate sub-annual climatic signals, rather than integrating a mean annual response given that rainfall intensity is often recognised as being of greater importance in erosion than rainfall amount alone (e.g. Nearing et al., 2004; Baartman et al., 2012). As such, the interpretation of these proxies is limited without further insight into the relationship between means and extremes.

Although the proxy record provides potentially important information on the hydrological cycle in a warm world, it can only

give a geographically-limited perspective, and it does not provide information on underlying mechanisms. However, modelling can provide context for local data, and can elucidate mechanisms. Despite this, there have not been any published modelling studies to date which have analysed changes in the global occurrence of extreme precipitation for the Eocene. The aims of this paper are (1) to use a GCM to investigate whether changes in the occurrence of precipitation extremes are simulated across the PETM; (2) to identify regions which are most likely to have been influenced by extreme, episodic precipitation events; and (3) to inform interpretation of proxy records by exploring the relationship between mean changes in precipitation and changes in precipitation extremes. In Section 2, we outline the modelling setup used for the PETM simulations. In Section 3, we characterise the occurrence of extreme precipitation events within the model for a series of Eocene-relevant model locations and develop global metrics for analysing spatial variations in extreme precipitation. In Section 4, we consider in detail the changes simulated at three case study locations, making comparisons with proxy data, and we also further discuss the ability of the model to represent precipitation extremes by comparison to preindustrial climate data, before drawing conclusions in Section 5.

2. Methods

The simulations in this paper are performed using HadCM3L, a fully-coupled atmosphere–ocean General Circulation Model (GCM), one of the suite of climate models developed by the UK Met Office (Gordon et al., 2000). HadCM3L has been used widely in the study of Eocene paleoclimate (Lunt et al., 2010; Loptson et al., 2014; Dunkley-Jones et al., 2013; Carmichael et al., 2017). Previous work in the context of future climate utilising HadCM3 – which operates at the same atmospheric resolution, but a higher oceanic resolution than HadCM3L – has shown that changes in the global precipitation frequency–intensity relationship, and therefore the increased occurrence of extremes, are seen in high CO₂ simulations (Allen and Ingram, 2002). The simulation of extreme precipitation events in the Indian monsoon region has also been investigated for future climate projections and has been shown to be related to Clausius–Clapeyron scaling (Turner and Slingo, 2009). However, extremes in the geological past have not been studied using this model.

The simulations presented here are initialised from those published by Loptson et al. (2014) to which the reader is referred for further details of model setup. Briefly, our equilibrium simulations are performed with atmospheric CO₂ at 2x and 4x preindustrial concentrations, utilising an early Eocene (~55 Ma) paleogeography (Lunt et al., 2010) and with a dynamically-evolving vegetation distribution (TRIFFID). Both the atmosphere and ocean modules operate on a grid of 2.5 degrees latitude by 3.75 degrees longitude and are resolved at a 30 minute time-step. In the nomenclature of Valdes et al. (2017), this model setup is described as HadCM3L-M2.1aD. The solar constant is reduced by 0.4% relative to modern day and the orbital configuration is set to preindustrial. Simulations were run for 99 model years, giving total integrations longer than 4000 model years. To study changes in occurrence of extreme events, precipitation rates were saved at every model hour for the 99 years. A preindustrial simulation with a modern-day land–sea mask was also performed at 1 × CO₂.

Within the simulations performed for this paper, the model-predicted global mean 1.5 m air temperatures increase from 18.99 °C in the 2 × CO₂ simulation to 24.00 °C in the 4 × CO₂ simulation, whilst global mean precipitation rate increases from 3.22 mm/day in the 2 × CO₂ simulation to 3.41 mm/day in the 4 × CO₂ simulation. The temperature anomaly between the new simulations discussed in this paper is therefore ~5 °C globally and

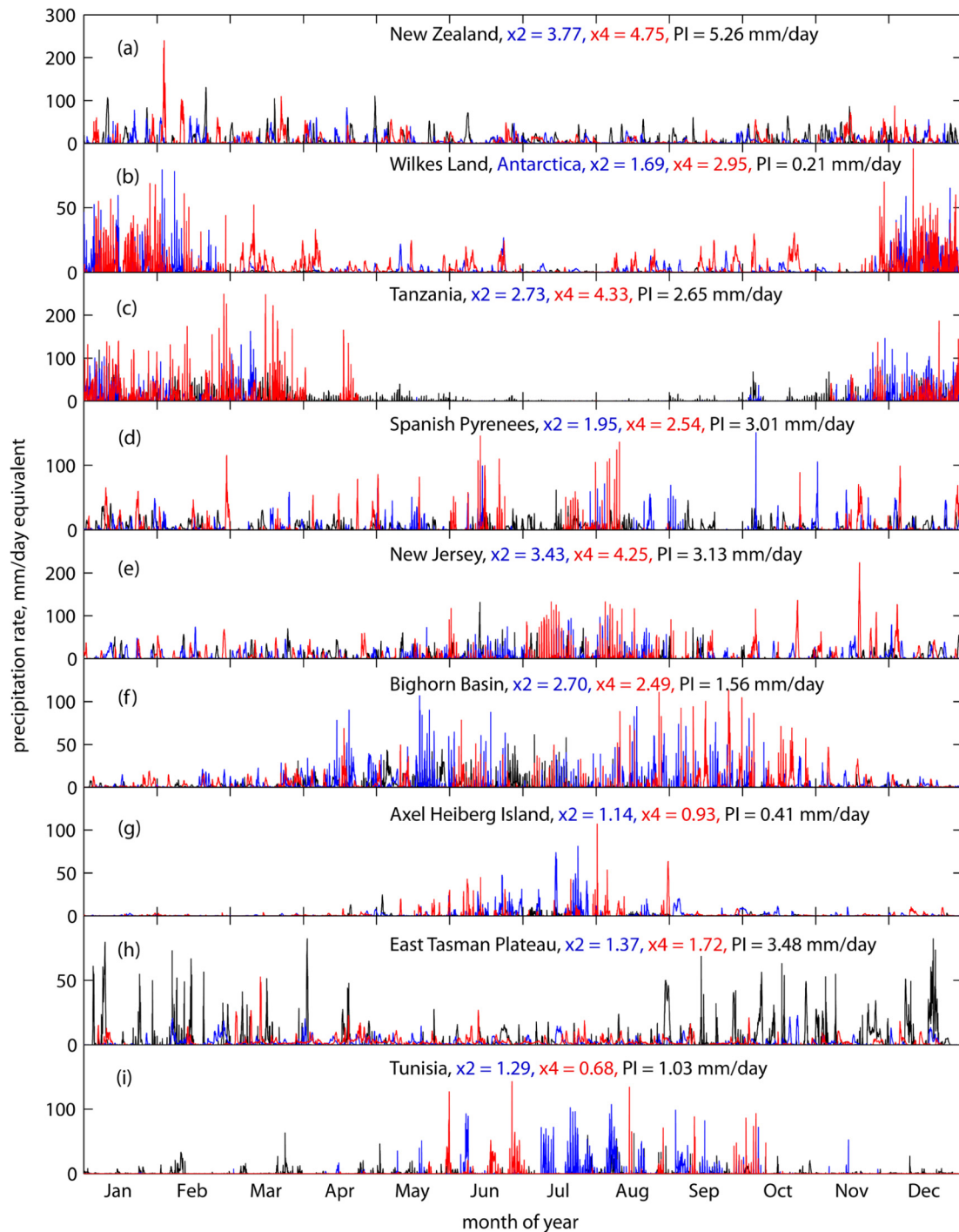


Fig. 1. Example model precipitation data at hourly resolution in the final year of the model simulations for preindustrial (black) and Eocene $2\times$ preindustrial CO_2 (blue, 'x2') and Eocene $4\times$ preindustrial CO_2 (red, 'x4') at single grid boxes corresponding to (a) New Zealand; (b) Wilkes Land, Antarctica; (c) Tanzania; (d) Spanish Pyrenees; (e) New Jersey margin; (f) Bighorn Basin; (g) Axel Heiberg Island; (h) East Tasman Plateau and (i) Tunisia. The mean annual precipitation rates in mm/day equivalent are also shown for each location in the upper right part of each plot. (For interpretation of the colours in the figure(s), the reader is referred to the web version of this article.)

approaches $\sim 8^\circ\text{C}$ in some high-latitude regions (Supplementary Fig. S1). This is of comparable magnitude to proxy-reconstructed estimates of surface temperature anomalies of the PETM relative to the pre-PETM (e.g. Dunkley-Jones et al., 2013 and references therein), despite model CO_2 being lower than some proxy estimates (Lunt et al., 2017). This study therefore represents a simple, idealised GCM experiment to assess how the occurrence of extreme precipitation could have changed between background early Eocene ($x2$) and PETM ($x4$) climate states.

3. Results

3.1. Comparing model-simulated Eocene and preindustrial precipitation regimes

Simulated hourly precipitation data from HadCM3L have not previously been considered within paleoclimatic studies. Examples of hourly GCM output for one year of the model simulations are therefore shown for illustrative purposes in Fig. 1 for a number of model locations at which either PETM or early Eocene precipita-

tion proxy data have been published. Note that the interpretations of changes in the hydrological cycle derived from these sites and their associated proxy data do not all include extreme behaviour (see Supplementary Information).

Since the primary aim of this paper is to explore how changes in extremes could influence the interpretation of proxy data, we focus on terrestrial grid cells representing likely hydrological impacts on terrestrial or marginal marine sites. These data represent the precipitation rate from the final year of the $x2$ (blue) and $x4$ (red) CO_2 Eocene simulations, along with a preindustrial simulation (black). Modern day locations of proxy data are rotated to their Eocene locations which means that differences between preindustrial and Eocene simulations are potentially due to both paleogeographic and climatic controls. Both preindustrial and paleo-model locations are provided in the Supplementary Information. These data illustrate that the model is capable of producing discrete events which may be considered extremes of the precipitation distribution. Maximum hourly precipitation rates are typically two orders of magnitude greater than mean annual precipitation rates, which are additionally indicated for each site on Fig. 1. Throughout this paper, all precipitation rates are stated in units of mm/day equivalent to allow comparison between mean annual, seasonal, daily and hourly precipitation rates (e.g. a rate of 5 mm/hour is stated as 120 mm/day equivalent).

The output from such time series indicates that modelled precipitation behaviour contrasts strongly in terms of duration, seasonality and intensity between the sites, both between sites for the Eocene and for the paleo-simulations relative to the preindustrial. Sensitivity to model boundary conditions is well illustrated for SE Australia regime (Fig. 1h), which is dominated in the preindustrial simulation by events which appear to last for a couple of days, whereas during the Eocene, events appear to be shorter, of reduced intensity and occur with a more equable seasonal distribution. These effects likely arise as a result of Australia being positioned about 25° further south compared to its present-day location, which is more monsoon-influenced (e.g. Huber and Goldner, 2012; Carmichael et al., 2016) and subject to larger summer convective storms.

Over Antarctica (Fig. 1b), the effects on precipitation rate of the elevated Eocene temperatures and absence of a continental ice sheet during the Eocene are clearly evident: mean annual precipitation in the $4 \times CO_2$ simulation is an order of magnitude larger than for the preindustrial, and intense short duration precipitation events are evident in austral summer, whilst the winter has lower intensity but longer lasting events relative to summer. The intense summer precipitation events over Antarctica relate to enhanced convection, whereas those of a longer duration in the winter appear to relate to the absence of a well-defined polar front in the Eocene and a less thermally isolated Antarctica, with greater influx of mid-latitude precipitation systems. The seasonal temperature control impact is also evident at Axel Heiberg Island in the Arctic (Fig. 1g).

A number of the sites show strong seasonality in the occurrence of intense precipitation events, but the reasons for this are complex. For example, at Tanzania, the preindustrial simulation appears to have a comparable mean annual precipitation rate to the $2 \times CO_2$ Eocene simulation, but during the Eocene the wet season is slightly shorter with more intense rates and almost no precipitation falls between May and October. The positioning of the ITCZ over Africa appears to be similar in the simulations, suggesting that this difference arises from the slightly more southerly position of Tanzania during Eocene, closer to the limit of ITCZ migration.

3.2. Spatial variations in the occurrence of extreme precipitation

Broadly, precipitation extremes represent the realisation of the right hand tail of the precipitation probability frequency distribution (Hartmann et al., 2013). However, a wide range of metrics exist by which to define an individual extreme event based on statistics of precipitation rate, frequency of occurrence and event duration (e.g. Zhang et al., 2011; Donat et al., 2013). Because this study is focused on identifying regions more liable to the effects of extremes at the PETM, it is necessary to compare regions with widely differing climatic regimes and so metrics based on absolute thresholds are avoided in favour of those which are dependent on precipitation statistics within each model grid box.

Our analysis is based on metrics which reflect model-simulated hourly precipitation rates. This is because a number of the existing proxies for changes in PETM hydrological regime tend to relate to variations in erosion, which may occur on hourly timescales, including sedimentation rate (John et al., 2008), export of terrestrial biomarkers (Handley et al., 2012) and kaolinite concentrations (Bolle and Adatte, 2001). Surface soil erosion is generally assumed to be controlled by rainfall drop impact with erosivity dependent on droplet velocity and size (e.g. Nearing et al., 2004). Due to these variables having characteristic timescales of minutes (Kandel et al., 2004), rainfall-runoff-erosion modelling typically utilises hourly or sub-hourly precipitation data where possible. A further rationale for examining extreme rainfall events on an hourly scale is that model-predicted hourly precipitation more effectively resolves peak event rainfall than daily precipitation. Supplementary Fig. S3 shows that intense events with high precipitation rates, but occurring over a short time interval, are often not well represented by daily precipitation totals. However, GCM-simulated sub-daily precipitation rates have received relatively little attention to date (e.g. Sun et al., 2006; Evans and Westra, 2012) and potential biases in the ability of GCMs to simulate realistic patterns must be considered (Section 5).

Fig. 2 characterises simulated changes in mean annual precipitation (a), and the incidence of extreme precipitation for a number of hourly metrics (b–d) across the PETM (i.e. $x4$ – $x2$ CO_2); all are shown as percentage changes and calculated from 99 years of hourly model data. Mean annual precipitation (MAP) shows strong increases in polar regions, associated with substantial temperature rise in these regions (Fig. S1). At lower latitudes, changes in MAP are highly variable for a given latitude. For example regions of both precipitation increase (Africa and India) and decrease (central America and South Asia) occur within equatorial regions, underlining the importance of comparing proxy data to model simulations and avoiding broad generalisations based on latitude. In some regions, changes in MAP at the PETM do not show substantial changes, despite indicators from the proxy record for hydrological change. For example, although a reduction in MAP is simulated within the western continental interior of the United States, this is $<10\%$, despite substantial changes in geomorphology within this region (Foreman et al., 2012). Tanzania is located close to the boundary of regions of increased and decreased precipitation change, despite significant increases in erosion and terrestrial biomarker delivery to continental margin (Handley et al., 2012).

The majority of the Eocene terrestrial surface experiences a decline in the total number of precipitation events from pre-PETM ($x2$ CO_2) to PETM ($x4$ CO_2) conditions, where an event is defined as any period with a consecutive non-zero precipitation rate (Fig. 2b). This reduction is particularly strong in Africa, the Amazon region and northern Australia with up to 30% fewer precipitation events. Such behaviour is consistent with the theoretical notion that precipitation intensity increases at a greater rate than total precipitation amount, at the expense of precipitation frequency (Trenberth, 2011; Sun et al., 2006). Some high-latitude regions

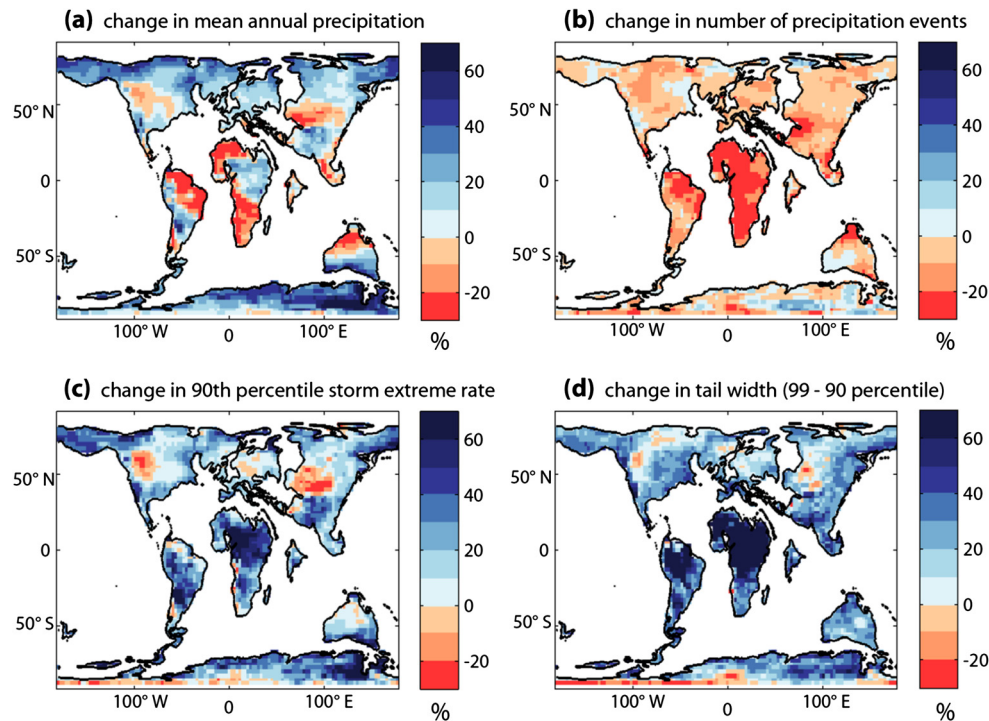


Fig. 2. Model simulated changes in precipitation across the PETM, calculated as a percentage change between $2 \times \text{CO}_2$ and $4 \times \text{CO}_2$ Eocene simulations for the following metrics (a) mean annual precipitation; (b) number of precipitation events occurring in 99 year sequence, where an event is defined as any period with consecutive non-zero precipitation rates; (c) 90th percentile value of the maximum precipitation rate attained in each individual precipitation event in the 99 year sequence; (d) tail width, defined by Scoccimarro et al. (2013) as the difference in rate between the 99th and 90th percentile precipitation rate.

including southern Australia, the Antarctic interior and isolated regions in the Arctic are an exception; these areas also generally experience a consistent increase in the percentage of time raining and mean annual precipitation. Aside from the high-latitude regions, the shift towards fewer rainfall events includes regions with both decreased and increased MAP. In regions where greater MAP is delivered to the Earth's surface in fewer precipitation events, there is an implied model-simulated shift towards either more intense events (i.e. increased precipitation rates; Fig. 2c), or more frequent heavy events of a given size (Fig. 2d).

For the purpose of this paper, extreme precipitation rate is defined as the 90th percentile value when considering the peak rainfall of each individual precipitation event within the 99 year time series. Most of the Earth's surface is characterised by increases in this value, indicating a near global increase in the intensity of the most extreme precipitation events; however, there are strong regional variations (Fig. 2c). An increase in this peak extreme rainfall by up to 70% occurs in tropical Africa, parts of South America and regions of the Arctic and Antarctic. More moderate changes are simulated for many mid-latitude regions, whereas declines in this precipitation rate are largely limited to continental interior regions of northern America and central Asia. However, these are both regions of decreased simulated mean annual precipitation, such that these changes may simply reflect shifts in the mean of the distribution as opposed to any true shift in the shape of the distribution. Furthermore, at high-latitude sites, there is a large increase in extreme precipitation rate – but similarly a $>60\%$ increase in MAP in these regions. This is not the case for all of the terrestrial surface, however, and there are regions where there is a model-simulated shift to more extreme precipitation rates without a corresponding change in MAP, for example subtropical Africa and Amazonia.

To further explore the changes in the relative importance of extreme precipitation, Fig. 2d shows the change in difference between the 90th and 99th percentile precipitation rates – a measure of the 'tailiness' of the distribution (Scoccimarro et al., 2013). In calculating this statistic, precipitation rates <1 mm/day equivalent

are excluded, to ensure that in regions where precipitation occurs regularly and at low intensity, the metric represents the distribution tail. In particular, these metrics indicate that extreme precipitation rates are quantitatively more important in the PETM simulation across much of the Earth's continental surface, but particularly so in equatorial regions, especially over Africa and western tropical regions of South America. The importance of convective mechanisms in governing extreme precipitation rates is further discussed within the Supplementary Information.

3.3. Seasonality of extreme precipitation events

The preceding analyses are based on hourly data from annual time series: events occurring in all months are incorporated into the calculations of the metrics. However, hydrological change can also be manifested as a shift in the seasonality of extreme precipitation or a differential response in precipitation rate between seasons. The Eocene simulations do not show major changes in the seasonal timing of the most extreme precipitation events across the PETM – i.e. the most extreme events trend to occur in the same months in both the pre-PETM and PETM simulations. Despite this, many terrestrial regions are characterised by strongly seasonal climates and although the timing remains similar, changes in the rate of extreme precipitation do show distinct seasonal responses, which could have important implications for proxy interpretation (Fig. 3).

The ratio of the summer to winter 90th percentile maximum event rate is shown for the $2 \times \text{CO}_2$ and $4 \times \text{CO}_2$ simulations in Fig. 3(a) and (b), respectively. This demonstrates the pronounced seasonality of precipitation extremes arising from the migration of the ITCZ in the tropics, whilst extremes are distributed more equably along the equator. Regimes dominated by more intense summer precipitation extremes also characterise eastern North America and Asia, South America and southern Africa. Although these seasonal distributions remain similar in the $4 \times \text{CO}_2$ simulation, few terrestrial regions show a year-round increase in the rate

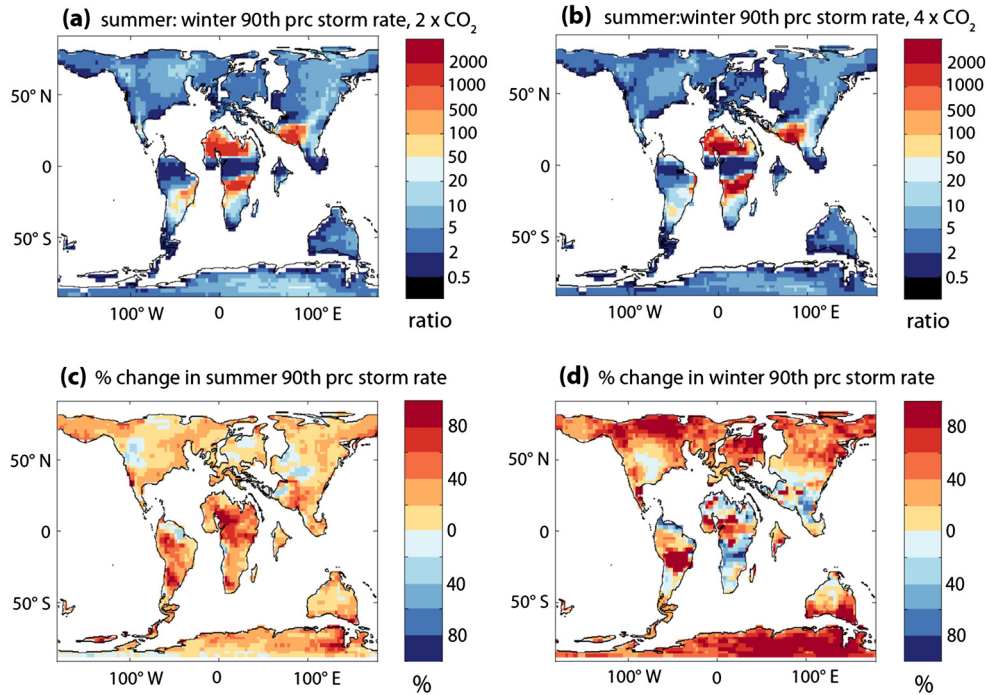


Fig. 3. Seasonal characterisation of precipitation extremes and change in the rate of extreme precipitation at the PETM. The ratio of 90th percentile maximum precipitation event rate summer to winter (JJA:DJF in Northern Hemisphere; DJF:JJA in Southern Hemisphere) is shown for the Eocene $2 \times \text{CO}_2$ simulation and $4 \times \text{CO}_2$ in (a) and (b) respectively. The percentage change in the 90th percentile maximum precipitation event precipitation rate between the $2 \times \text{CO}_2$ and $4 \times \text{CO}_2$ simulations are shown in (c) and (d).

of extreme precipitation – those which do tend to be the high latitudes (Fig. 3c and d). Regions which show the largest seasonal contrast include south west Asia, northern Africa and particularly tropical East Africa, where winter 90th percentile maximum precipitation event rates show declines, whilst the summer rates increase.

4. Discussion

The results of the simulations provide a modelling framework with which to examine hypotheses derived from proxy studies for changes to hydrological regimes at the PETM. Three examples are discussed in detail below (Section 4.1). Because of the relatively coarse resolution of HadCM3L, the focus is on locations where large-scale signals appear to be evident in the model output (Fig. 2). It is also possible to use the simulations to identify regions which could be more likely to record a response in extreme precipitation behaviour (Section 4.2). This includes regions where the change in the occurrence of precipitation extremes is large across the PETM, but the change in mean annual precipitation is small or declines at the PETM. We additionally consider the degree to which HadCM3L adequately represents extreme precipitation behaviour (Section 4.3).

4.1. Interpreting existing paleoclimate data from the PETM

4.1.1. Tropical Africa

Low-latitude terrestrial sites are scarce for the early Eocene. However, sediments from the Tanzanian Drilling Project (Pearson et al., 2004) have yielded insights into the hydrological response of tropical East Africa at the PETM. Compound specific isotope analysis was performed on *n*-alkane biomarkers of a putative leaf-wax origin by Handley et al. (2012), who observed an enrichment of $>30\%$ in the $\delta^2\text{H}$ value of C_{31} *n*-alkane, corresponding to the onset of the PETM. In addition, there is a significant increase in the transport of terrestrially-derived biomarkers, quartz and kaolinite from the continental interior to the outer shelf depositional setting. Because of the low latitude location ($\sim 12^\circ\text{S}$ paleolatitude), with a

vapour source close to VSMOW, the authors suggested deuterium enrichment was unlikely to have been produced by a change in vapour source and could not be fully accounted for by the effects of regional temperature changes on vapour fractionation. Whilst there are a range of caveats in this interpretation (e.g. Costa et al., 2014 and Sachse et al., 2012), the enrichment was interpreted as reflecting an increase in aridity, with elevated evaporation causing a $\delta^2\text{H}$ enrichment in soil or leaf water. To rationalise this interpretation with increased input of terrestrial biomarkers and kaolinite, the authors inferred that rainfall over tropical East Africa became more episodic and extreme at the PETM, or perhaps occurred with a more seasonal distribution.

Our climate simulations support this interpretation. The extreme seasonality of the precipitation influencing the Tanzanian site is shown in Fig. 1 and Fig. 3; this variation is a result of the seasonal migration of the Inter-Tropical Convergence Zone (ITCZ). The simulations do not indicate significant changes to MAP or to the seasonal precipitation distribution between pre-PETM and PETM conditions, the former increasing by just 0.71% and the latter showing a 4.01% decline in DJF (Fig. 4). Furthermore, the dry season remains similar in length in the $4 \times \text{CO}_2$ simulation; for example, the longest consecutive period with daily averaged precipitation not exceeding 1 mm/day falls from 198 days/year in the $2 \times \text{CO}_2$ simulation to 195 days/year in the $4 \times \text{CO}_2$ simulation. However, the rate of extreme precipitation is particularly sensitive over much of tropical Africa, with an increase in the occurrence of extreme precipitation rate in the wet season such that the intra-annual contrast is increased (Fig. 4). For example, the 90th percentile maximum precipitation event rate increases in the DJF season from 82.6 mm/day equivalent in the $x2$ simulation to 100.4 mm/day in the $x4$ simulation, whilst that of the 99th percentile increases from 146.8 to 189.1 mm/day. Fig. 5 shows the change in the shape of the precipitation probability distribution for this site, with precipitation rates greater than 80 mm/day equivalent occurring more frequently in the $4 \times \text{CO}_2$ simulation, and events

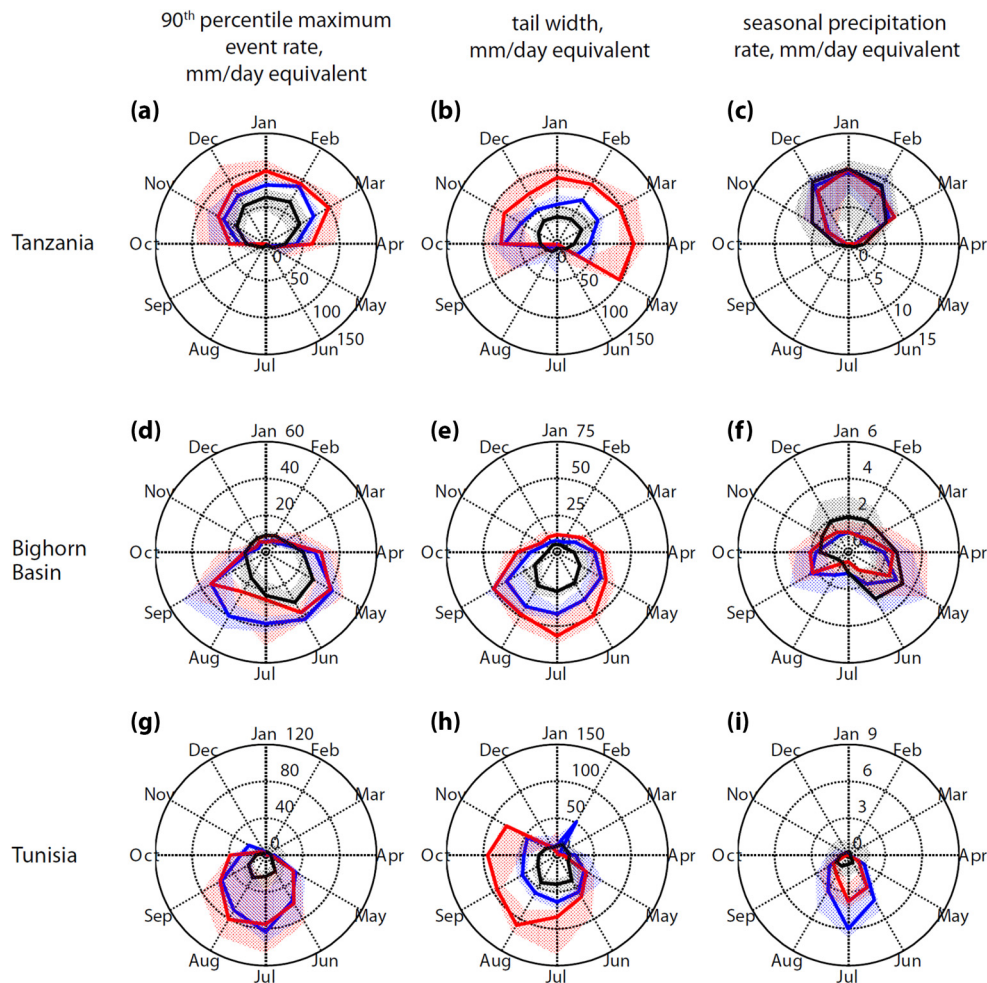


Fig. 4. Changes in extreme and seasonally averaged precipitation rates for model grid boxes corresponding to (a, b, c) Tanzania; (d, e, f) Bighorn Basin, Wyoming; (g, h, i) Tunisia. The Eocene simulation at $2 \times \text{CO}_2$ is shown in blue, $4 \times \text{CO}_2$ in red and corresponding preindustrial simulation and location at $1 \times \text{CO}_2$ in black. Panels a, d, g show the extreme precipitation rate, calculate as the 90th percentile maximum precipitation event rate; b, e, h show the tail width, calculated as the difference between 99th and 90th percentile precipitation rate; c, f, i show the seasonal precipitation rates. The shaded regions show the corresponding minimum and maximum values for each of the metrics calculated from the 8 grid boxes surrounding the location of interest.

larger than 200 mm/day equivalent occurring an order of magnitude more frequently.

Calculations within the Supplementary Information indicate that this region may have been subject to enhanced aridity during the PETM. Increased aridity could have exacerbated the impact of extreme precipitation change on erosion and contributed to the sedimentological changes documented in Tanzanian sediments, either through vegetation or soil organic matter feedbacks or through more direct effects of drying on soil structure. Moreover, similar changes occur in other tropical regions between pre-PETM and PETM conditions (Fig. 2). Therefore, it is possible that increased evapotranspiration and drying of the soil, coupled to more intense precipitation events, resulted in dramatically increased tropical erosion at the PETM.

4.1.2. Northern Africa and Tethys Ocean

Many other marginal marine PETM sections are characterised by elevated sedimentation rates relative to the background Eocene climate, with increases by an order of magnitude at many sites around the Peri-Tethyan Sea including modern day Spain, Italy, Kazakhstan and Uzbekistan on the northern margin, and Tunisia and Egypt on the southern margin (John et al., 2008; summary in Carmichael et al., 2017). Changes in sedimentation have been interpreted to reflect increased weathering as a result of an intensified hydrological cycle, although the climatic signal causing

these changes has not been fully investigated. However, a decline in mean annual precipitation is simulated within the Eocene simulations along the northern Africa coastline, driven by consistent declines in precipitation between May–October (Fig. 4). At Tunisia, the decline in mean annual precipitation is around 35%, suggesting that the elevated PETM sedimentation rates along the southern Tethys margin are unlikely to have been caused by increased weathering relating to changes in annual or seasonal precipitation distributions.

The Eocene simulations allow a more nuanced interpretation of hydrological change in this region that can potentially help explain the observed increase in sedimentation rates. Despite a fall in convective precipitation (Supplementary Fig. S4), Tunisia is located within the subtropics, where precipitation is nearly unanimously convective in nature, rather than frontal. Furthermore, the region experiences large temperature changes and subsequent increases in specific humidity. Dynamical mechanisms may also play a role – the north-easterly originating trade winds blow onshore from the Tethys Ocean where specific humidity and wind strength both increase in the $4 \times \text{CO}_2$ simulation. Although changes in the absolute rate of 90th percentile maximum event precipitation are muted at this location (Fig. 4), with only minor increases apparent between August–October, the convergence of the above factors result in a precipitation distribution that is consistently more ‘tailly’ between July and November, with a shift occurring in the shape of the pre-

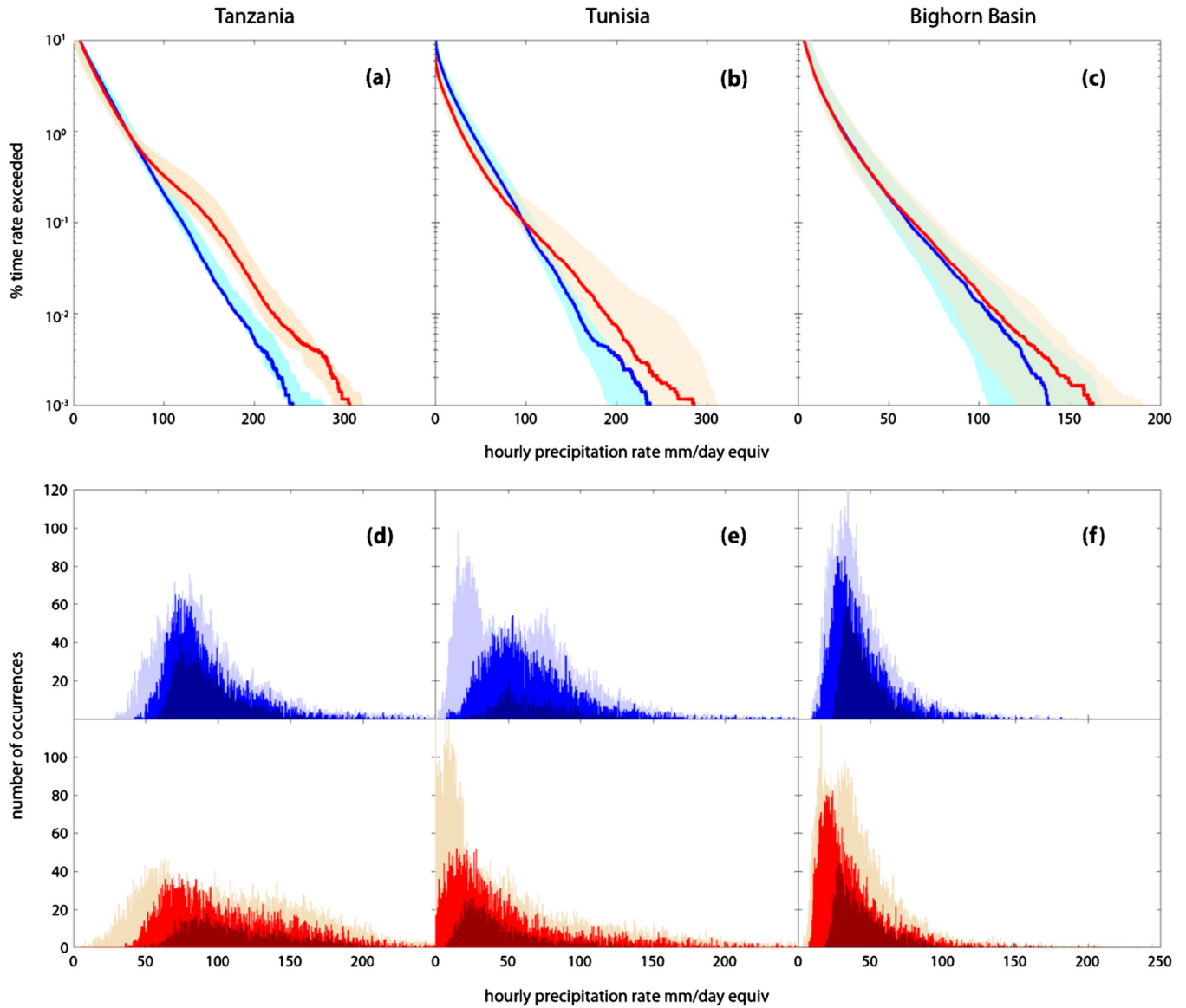


Fig. 5. Model simulated PETM changes in precipitation frequency distribution at Tanzania (a, d), Tunisia (b, e) and Bighorn Basin (c, f) for $2 \times \text{CO}_2$ (blue) and $4 \times \text{CO}_2$ (red) simulations. The top row of panels (a–c) show the percentage of time a given precipitation rate is exceeded in the 99 years of simulations, whilst the bottom panels (d–f) show a histogram of the largest 50 precipitation events of each of the 99 years with a bar width of 1 mm/day on the x-axis. The shading in (a–c) and (d–f) shows the corresponding minimum and maximum values calculated from the 8 grid boxes surrounding the location of interest.

precipitation distribution (Fig. 5). The simulations therefore indicate that the occurrence of extreme precipitation could have been a cause of enhanced erosion at this site. Lighter precipitation events, below around 100 mm/day equivalent are reduced in occurrence in the $4 \times \text{CO}_2$ simulation, whilst events larger than this become more commonplace, although rare (Fig. 5). For example, a precipitation event which attains a precipitation rate of 180 mm/day equivalent has a recurrence interval of ~ 2.4 years in the $2 \times \text{CO}_2$ simulation and this is reduced to ~ 0.94 years in the $4 \times \text{CO}_2$ simulation.

Other factors may also play a role, alongside or acting independently of the occurrence of extreme precipitation. Simulated evapotranspiration decreases within this region (Loftson et al., 2014), resulting in elevated P–E and therefore implying increased runoff – by as much as 88% – which could be responsible for greater sediment delivery to the continental margin. Secondly, the model simulations of Loftson et al. (2014) also indicate vegetation changes at the PETM along the northern margin of Africa. In particular, equatorial Africa is dominated by non-forest cover in the pre-PETM $2 \times \text{CO}_2$ simulation. The simulations show a strong increase in bare

soil cover in PETM $4 \times \text{CO}_2$ simulation, increasing from around 19% to 75% at Tunisia, perhaps implying that this region was particularly exposed to increased soil erosion (Fig. 6). The interaction of these processes requires further study; for example, the change in vegetation cover likely resulted from increased water stress imposed by elevated evapotranspiration rates (Loftson et al., 2014; Hunter et al., 2013). Nonetheless, the combination of more extreme events, greater runoff and an increase in bare soil cover suggested by the simulations could account for changes in sedimentation rate observed along the southern Peri-Tethyan margin.

4.1.3. Continental United States

The Bighorn Basin is one of the best-studied terrestrial PETM sites, with vertically stacked paleosols providing high-resolution insights into hydrological and related environmental changes. Initially, an increased terrestrial Carbon Isotope Excursion (CIE) at the PETM was suggested to indicate more humid and wetter conditions (Bowen et al., 2004), but deuterium isotopes of *n*-alkanes and pronounced cyclic changes in paleosol characteristics indicate

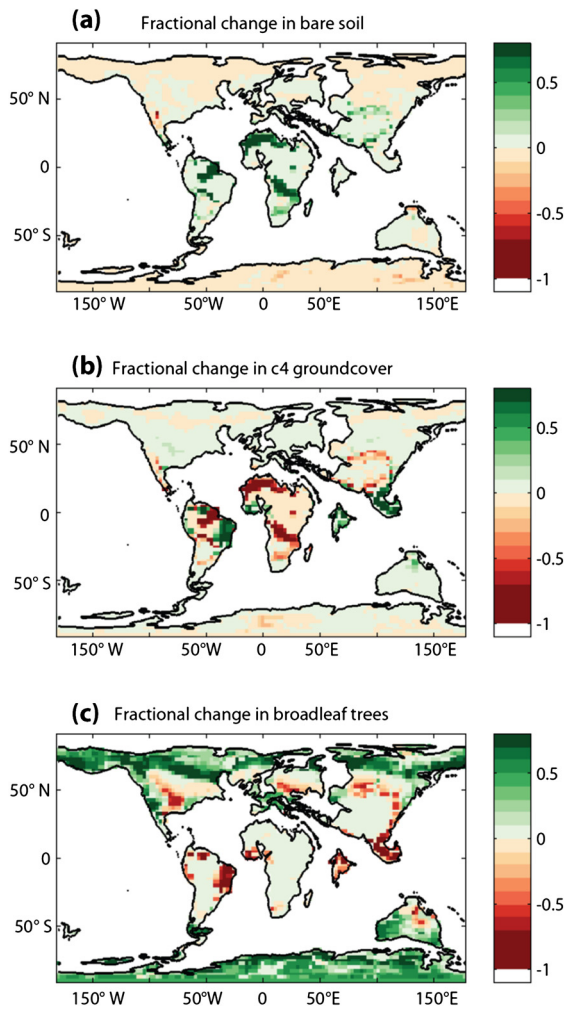


Fig. 6. Changes in the simulated fraction cover of vegetation in the HadCM3L simulations of Loptson et al. (2014), $4 \times \text{CO}_2$ – $2 \times \text{CO}_2$. Surface cover changes are shown for (a) bare soil (b) C_4 groundcover, equivalent of non-forest vegetation and (c) broadleaf forests.

fluctuations in the regional hydrology throughout the event (Smith et al., 2007; Kraus et al., 2013). By comparison to late Paleocene leaf fossils, a decline in precipitation of $\sim 40\%$ has been suggested at the onset of the PETM, with recovery to pre-onset values by the end of the event (Wing et al., 2005). Whilst paleosols suggest transitional climatic changes, they generally indicate a progressive drying within the body of the PETM (Kraus et al., 2013), although these changes are complex with drying occurring prior to the CIE onset and a recovery to wetter soils which persists after the CIE recovery. Support for this initial drying is provided by the distribution of floodplain ichnofossils (Smith et al., 2008) and floral assemblage data (Kraus et al., 2013). In contrast, the development of a sandstone boundary stone and geomorphological changes are consistent with high discharge river flows, and are perhaps indicative of more flashy hydrological regimes (Foreman et al., 2012). However, the potential for these different proxies to incorporate regional hydrological signals on different timescales has not previously been considered in GCMs.

The simulations show complex behaviour within the US continental interior. Mean annual precipitation does decrease in the $4 \times \text{CO}_2$ simulation, but by only 5.5% relative to the $2 \times \text{CO}_2$ simulation. However, summer season (JJA) precipitation decreases by 48.4% (Fig. 4), which could disproportionately impact proxy responses – particularly those based on the leaf physiognomy or pollen composition that record a growing season signal. Al-

though the 90th percentile maximum rate suggests a reduction in the occurrence of extreme precipitation rates at this location (Fig. 2), analysis of the distribution tail (Fig. 5) shows that the rarer most intense events do also occur more frequently in the high CO_2 simulation; for example, a precipitation rate which exceeds 140 mm/day equivalent occurs with a recurrence interval of ~ 11 years in the $2 \times \text{CO}_2$ simulation but ~ 3.5 years in the $4 \times \text{CO}_2$ simulation. This apparent contradictory behaviour may be explained by the observation that precipitation events affecting continental interior US are generally regular, low intensity events, such that the 90th percentile maximum event rate does not necessarily reflect a particularly ‘rare’ event (Fig. 1f). This underscores the difficulty in defining *a priori* the size of a precipitation extreme which is of the greatest relevance to interpreting the proxy record. Although there is growing recognition that extreme precipitation rates are important controls on biota, reduced seasonal precipitation likely dominates floodplain water table conditions impacting ichnofossil distribution and plant distributions. Conversely, annual maximum bankfull discharge conditions have been suggested to be important in governing geomorphological changes and the development of the boundary sheet sandstone could relate to the increased occurrence of very rare intense events in the $4 \times \text{CO}_2$ simulation. Therefore, the different proxies described for the Bighorn Basin are not necessarily contradictory, but rather may be reflecting different time-averaged signals precipitation (or other hydrological) signals.

The degree to which the changes inferred from proxies from the Bighorn Basin are typical of continental interiors is subject of interest given the scarcity of terrestrial sections for the PETM. The simulations of Loptson et al. (2014) indicate that despite the relatively large increases in terrestrial temperatures, the smallest global increases in specific humidity occur within the Western US, which is likely due to the extreme continentality of this region. This may explain the differing behaviour between very rare extremes and mean annual precipitation behaviour. The continental interior of China also shows a muted change in specific humidity, perhaps suggesting that similar changes could have affected this region. However, for a given latitude, there is a wide model spread in hydrological response (e.g. Fig. 2c and d), underlining the need for further proxy data from terrestrial regions to ‘ground truth’ simulations.

4.2. Global interpretations and proxy acquisition

The simulations presented in this paper only suggest an alternative explanation for elevated sedimentation rates and proxies sensitive to erosion; it is not possible to discriminate between the effects of extreme precipitation, changes in runoff or vegetation cover. However, our analysis indicates that many regions show decoupled changes in means and extremes, on account of the differing controlling processes (Section 1). This includes regions where mean annual precipitation declines, but increases occur in the ‘tailiness’ of the distribution, or incidence of extreme precipitation rates. Such regions are highlighted within our summary Fig. 7.

Climate model simulations can be utilised to provide insights into locations for obtaining climate proxy data, including where there is a high simulated signal-to-noise ratio, or where model simulations show considerable spread (e.g. Lunt et al., 2008; Comboul and Emile-Geay, 2015). We suggest that the regions shown in Fig. 7 represent important targets for proxy acquisition with the potential to contribute further to understanding the effects of extremes on sedimentary responses, in the absence of increases or substantial changes in annual precipitation amount. High latitude regions are generally characterised by increases in both mean annual and extreme precipitation – as such, it is more difficult to attribute hydrological causes of proxy responses.

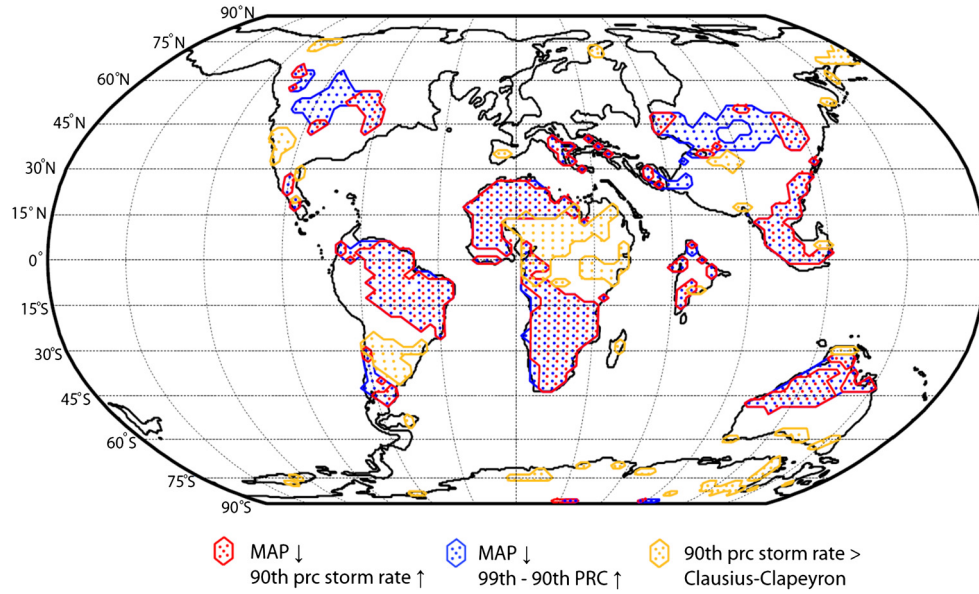


Fig. 7. Schematic for proxy acquisition to investigate the effect of extreme precipitation at the PETM. Blue shaded areas are regions where mean annual precipitation declines but precipitation distribution 'tailiness' increases; red shaded areas are regions where mean annual precipitation declines but 90th percentile maximum event rate increases. Gold shaded areas are regions which have an increase in the 90th percentile maximum event rate which exceeds the thermodynamic Clausius–Clapeyron scaling for the local temperature change (details provided in Supplementary Information).

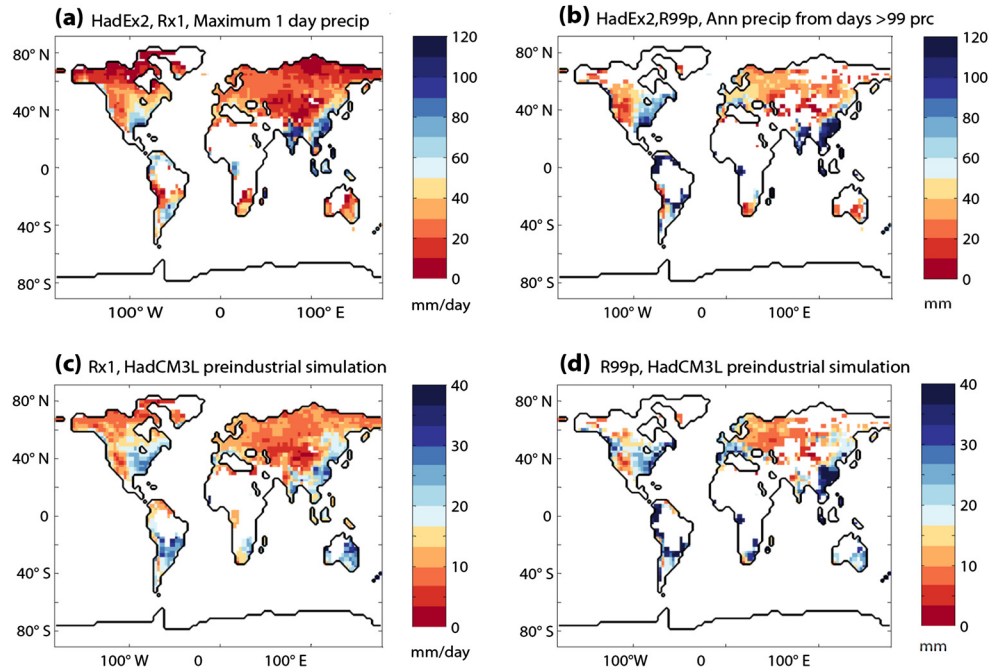


Fig. 8. Comparison of daily extreme precipitation metrics of the HadEx2 dataset (Donat et al., 2013) to the preindustrial model simulation; (a) and (c) show Rx1, the maximum annual daily precipitation rate and (b) and (d) show R99p, the 99th percentile daily precipitation rate. Note the different scales for the observational and model simulated data.

4.3. How well does HadCM3L represent extremes?

Although changes in the occurrence of extremes in a warm climate state are expected from thermodynamics, the tail of the precipitation frequency distribution is challenging for GCMs to simulate, especially for relatively low-resolution models. As such, analysis of regional variability in extreme characteristics would benefit from model validation. This is not straightforward given that observational data of extreme precipitation rates are rare; where data do exist, time series are often short and unlikely to sample full natural variability and they are limited in their spatial coverage. The HadEx2 dataset (Donat et al., 2013) provides gridded modern-day

observations of a range of daily extreme temperature and precipitation characteristics on the same $3.75^\circ \times 2.5^\circ$ latitude–longitude grid as the Eocene and preindustrial model simulations. This represents one of the most comprehensive estimates for observational data, but for some precipitation metrics the coverage is less than 40% of the terrestrial surface.

In Fig. 8, two observational metrics for extreme precipitation – the maximum annual 1 day precipitation rate (Rx1) and the contribution to MAP of days above the 99th percentile rate (R99p) are compared with the preindustrial $1 \times \text{CO}_2$ HadCM3L simulation. In both cases, the spatial variation in the indices suggest that the model performs relatively well at simulating relative differences

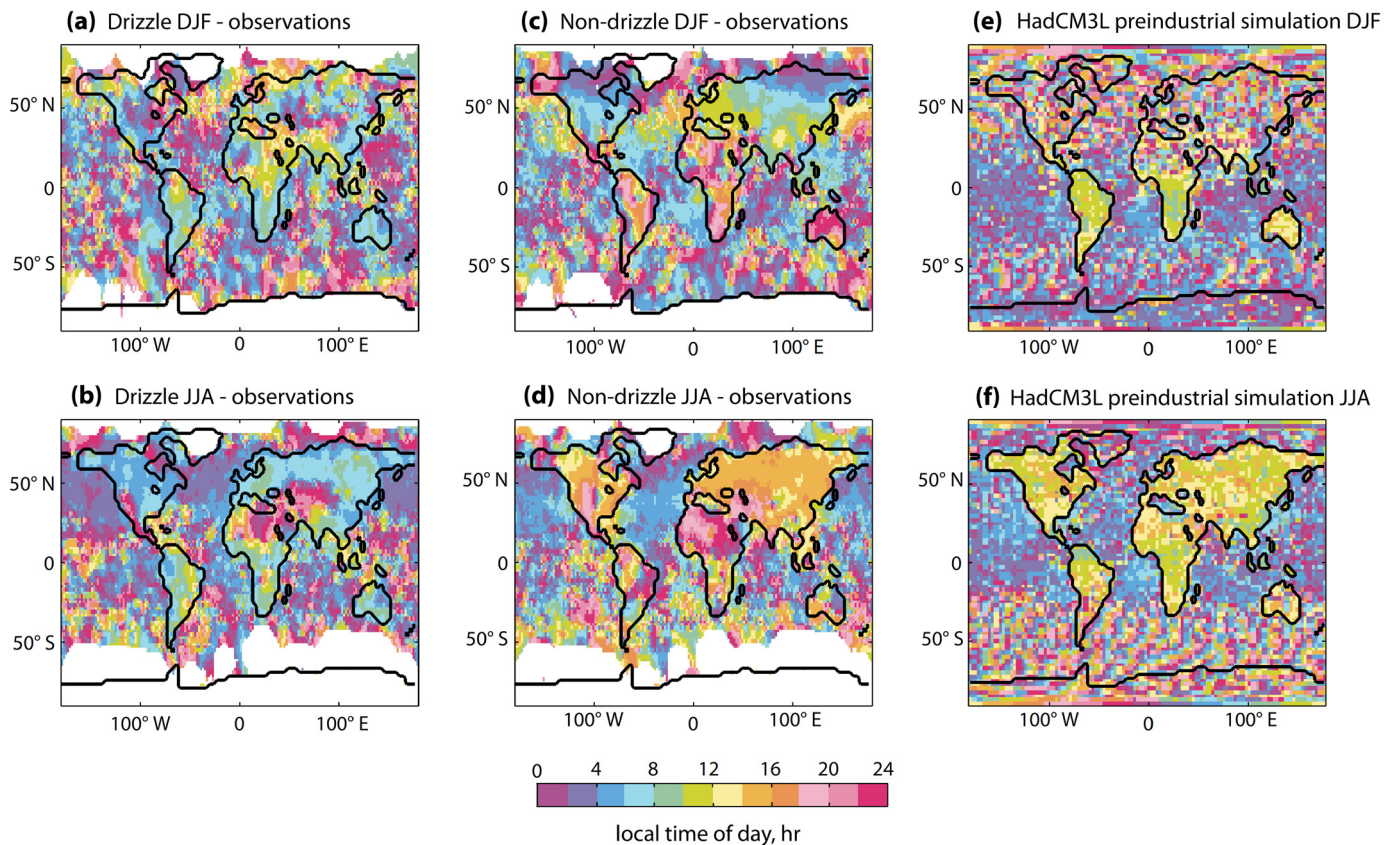


Fig. 9. Observed and simulated local time of maximum daily precipitation rate for JJA (a, b, c) and DJF (d, e, f) seasons. Observed data are categorised as drizzle (a, d) and non-drizzle (b, c) and observational data are from Dai (2001). Although the simulated precipitation has not been categorised as drizzle or non-drizzle, this is unlikely to impact on the spatial pattern, given that the plot is based upon the timing of the maximum daily rate. Whilst the winter hemisphere displays a more ‘granular’ pattern with apparently more random timing of the most intense events within the model simulation, the majority of the terrestrial surface, particularly in JJA, shows a peak in precipitation consistently occurring between 10 AM and 3 PM, whereas the observational data show much greater spatial heterogeneity in this value.

across the Earth’s surface. However, the model does a much poorer job in the simulation of the absolute precipitation rates associated with the extreme ‘tail’ of the distribution. Maximum model simulated values are typically around a third of the observational values. Therefore, percentage change plots or qualitative interpretations (e.g. Figs. 2, 3) may be more robust than absolute rates (e.g. Fig. 4).

Two main groups of reasons may explain why the model underestimates the magnitude of absolute extreme precipitation rates: (1) grid resolution and (2) model parameterisations. In the case of the former, different methods for comparing point-wise (station, gauge) estimates of extreme precipitation to those resolved on a coarse model grid remain largely untested (e.g. Gervais et al., 2014; Chen and Knutson, 2008). By their very nature, extreme events are very localised and discontinuous. Although the HadEx2 dataset is based on ~11300 precipitation gauge data which are interpolated to a regular grid (Donat et al., 2013), whether these data are truly comparable to model data is highly uncertain; Chen and Knutson (2008) found that differences of up to 30% in daily averaged extreme precipitation rates occurred over the United States, according to interpolation scheme and whether GCM precipitation was considered to represent a point estimate or areal average rate. Furthermore, dynamical features associated with extremes (e.g. storm tracks) are in general better represented in high resolution models than in low resolution models (Willison et al., 2015).

In the case of the latter, it is widely assumed that the most extreme precipitation events are those arising from convective precipitation rates (Section 3.2; Supplementary Information), which are therefore reliant on the convective parameterisation scheme implemented within the GCM. Early onset of daytime moist con-

vection is a well-studied phenomenon in GCMs (Ban et al., 2015; Dai and Trenberth, 2004), which results in model precipitation occurring too frequently – the so called ‘constant drizzle’ problem. This prevents a build-up of convective potential energy and may thereby account for the reduced intensity of precipitation events. This again suggests that absolute rates (e.g. Fig. 4) are likely to be less reliable than the relative percentage changes (e.g. Figs. 2 and 3). This effect is illustrated in Fig. 9, where the maximum local time of diurnal precipitation in the preindustrial $1 \times \text{CO}_2$ simulation is shown, relative to the observations of Dai (2001). This demonstrates a bias within HadCM3L, whereby maximum precipitation typically occurs in all terrestrial regions between 10 AM and 3 PM, whilst observational data suggest greater spatial heterogeneity. A comparison of CMIP5 simulations, also to the HadEx2 dataset, has shown that state-of-the-art GCMs continue to suffer from an underestimation of extreme precipitation values (Asadieh and Krakauer, 2015).

Higher resolution cloud resolving models (CRMs) and superparameterised models which explicitly resolve moist convection have had some success in better simulating the distribution of intense precipitation events relative to standard GCMs (Li et al., 2012; Ban et al., 2015). A natural progression from a global approach here would therefore be to study the occurrence of extremes in these newer models; the computational requirement of running such a model at this additional level of complexity would necessitate a regional approach. Furthermore, several of the regions of considerable discrepancy between the HadEx2 data and model simulations are in mountainous regions (Rockies; Himalayas; Andes) or those with complex seasonal atmospheric circulations, such as monsoon regions (Indian subcontinent; central America). Given

the low resolution atmospheric representation within HadCM3L and difficulties of simulating accurate moisture gradients (e.g. Valdes et al., 2017), a regional model approach (e.g. HadRM3B) could prove beneficial to test the robustness of our results. As such, this study has highlighted regions where a decoupling of the MAP signal and extremes takes place which could serve as target regions.

5. Conclusions

The simulations presented in this paper provide support for a shift in frequency–intensity of precipitation distributions at the PETM, as has been hypothesised from recent Eocene proxy studies. In the majority of terrestrial regions, HadCM3L simulates a shift to higher intensity of extreme precipitation and a decline in the overall number of precipitation events. The simulations provide support for extreme precipitation increasing in importance during the PETM within tropical and subtropical Africa and parts of South America, whilst at high latitudes increases in both mean annual precipitation and extreme rates are found.

Despite shortcomings in the representation of extreme rates, the simulations illustrate that changes in the occurrence of extreme precipitation can be decoupled from changes in mean annual precipitation, and hydrological change is manifested as a change in the shape of the precipitation distribution. This includes regions where the incidence of extreme events increase, but mean annual precipitation remains relatively constant (e.g. Tanzania) or declines (e.g. Tunisia). This has implications for undertaking proxy-model comparisons, because different proxies likely incorporate these different climatic signals. Existing proxy-model comparisons for warm climate states which compare proxy responses to mean annual signals alone (e.g. Carmichael et al., 2017) may therefore be limited, particularly in the low and mid-latitudes.

The robustness of the results presented here does require further testing with other climate models and the sensitivity of the results to model boundary conditions and parameterisation schemes should also be investigated. This is particularly important given the possible model-specific Eocene mean annual responses identified in Carmichael et al. (2016), which included differences in both the Bighorn Basin and equatorial Africa in HadCM3L and CCSM3, models of similar atmospheric resolution. Caution is also required given the long-standing problems of Eocene high-latitude cold model biases (e.g. Huber and Caballero, 2011) and the systematic low latitude biases – for example simulation of ITCZ structure and seasonality – apparent in preindustrial model simulations (Carmichael et al., 2016).

Although the spatial patterns described here are specific to Eocene boundary conditions, it is noteworthy that there are several similarities between simulated PETM behaviour and future predicted precipitation change. Scoccimarro et al. (2013), using a CMIP5 RCP8.5 forcing, simulated widespread increases in future predicted tail width (albeit for daily statistics). Particularly acute changes of more than 50% are predicted within equatorial Africa and South East Asia between June–August, although seasonal variations were apparent. Their study also demonstrates that the occurrence of the rarest events can differ markedly from other measures of the distribution; over larger regions of North America and Europe, 90th percentile precipitation rates decline, despite small increases in tail width. Further comparisons of metrics utilised for future climate studies with paleoclimate simulations could assist in identifying changes that are common to warm climate periods.

Despite the shortcomings outlined, Earth system models lend support to interpretations of hydrological proxies via their simulation of both climatic parameters and land surface parameters, the synergistic effects of which are also important targets for future research. Models therefore have a critical role to play in helping

'decode' differing proxies in the interpretation of the geological record and we advocate that future paleoclimatic modelling pays explicit attention to the occurrence of extreme events, in addition to changes simulated on mean annual and seasonal timescales.

Acknowledgements

This work was carried out using the computational facilities of the Advanced Computing Research Centre, University of Bristol – <http://www.bris.ac.uk/acrc/>. The research leading to these results has received funding from the European Research Council Grant Agreement number 340923 (The Greenhouse Earth System, T-GRES, awarded to RDP). RDP acknowledges the Royal Society Wolfson Research Merit Award. DJL acknowledges NERC grant CPE (NE/K012479/1).

Appendix A. Supplementary material

Supplementary material related to this article can be found online at <https://doi.org/10.1016/j.epsl.2018.08.005>. Hourly simulated precipitation data for the sites discussed in the text can be obtained by emailing the corresponding author.

References

- Allen, M.R., Ingram, W.J., 2002. Constraints on future changes in climate and the hydrologic cycle. *Nature* 419 (6903), 224–232.
- Asadieh, B., Krakauer, N.Y., 2015. Global trends in extreme precipitation: climate models versus observations. *Hydrol. Earth Syst. Sci.* 19, 877–891.
- Baartman, J.E.M., Jetten, V.G., Ritsema, C.J., de Vente, J., 2012. Exploring effects of rainfall intensity and duration on soil erosion at the catchment scale using openLISEM: Prado catchment, SE Spain. *Hydrol. Process.* 26, 1034–1049.
- Ban, N., Schmidli, J., Schar, C., 2015. Heavy precipitation in a changing climate: does short-term summer precipitation increase faster? *Geophys. Res. Lett.* 42, 1165–1172.
- Bolle, M.P., Adatte, T., 2001. Palaeocene early Eocene climatic evolution in the Tethyan realm: clay mineral evidence. *Clay Miner.* 36 (2), 249–261.
- Bowen, G.J., Beerling, D.J., Koch, P.L., Zachos, J.C., Quattlebaum, T., 2004. A humid climate state during the Paleocene/Eocene thermal maximum. *Nature* 432, 494–499.
- Carmichael, M.J., Lunt, D.J., Huber, M., Heinemann, M., Kiehl, J., LeGrande, A., Loptson, C.A., Roberts, C.D., Sagoo, N., Shields, C., Valdes, P.J., Winguth, A., Winguth, C., Pancost, R.D., 2016. A model–model and data–model comparison for the early Eocene hydrological cycle. *Clim. Past* 12 (2), 455–481.
- Carmichael, M.J., Inglis, G.N., Badger, M.P.S., Naafs, B.D.A., Behrooz, L., Rimmelzwaal, S., Monteiro, F.M., Rohrsen, M., Farnsworth, A., Buss, H.L., Dickson, A.J., Valdes, P.J., Lunt, D.J., Pancost, R.D., 2017. Hydrological and associated biogeochemical consequences of rapid global warming during the Paleocene–Eocene Thermal Maximum. *Glob. Planet. Change* 157, 114–138.
- Chen, C.T., Knutson, T., 2008. On the verification and comparison of extreme rainfall indices from climate models. *J. Climate* 21, 1605–1621.
- Comboul, M., Emile-Geay, J., 2015. Paleoclimate sampling as a sensor placement problem. *J. Climate* 28, 7717–7739.
- Costa, K.M., Russell, J., Konecky, B., Lamb, H., 2014. Isotopic reconstruction of the African Humid Period and Congo air boundary migration at Lake Tana, Ethiopia. *Quat. Sci. Rev.* 83, 58–67.
- Dai, A., 2001. Global precipitation and thunderstorm frequencies. Part II: diurnal variations. *J. Climate* 14, 1112–1128.
- Dai, A., Trenberth, K.E., 2004. The diurnal cycle and its depiction in the community climate system model. *J. Climate* 17, 930–951.
- Dittus, A.J., Karoly, D.J., Lewis, S.C., Alexander, L.V., 2015. A multiregion assessment of observed changes in the areal extent of temperature and precipitation extremes. *J. Climate* 28, 9206–9220.
- Donat, M.G., Alexander, L.V., Yang, H., Durre, I., Vose, R., Dunn, R.J.H., Willett, K.M., Aguilar, E., Brunet, M., Caesar, J., Hewitson, B., Jack, C., Klein Tank, A.M.G., Kruger, A.C., Marengo, J., Peterson, T.C., Renom, M., Oria Rojas, C., Rusticucci, M., Salinger, J., Elayah, A.S., Sekele, S.S., Srivastava, A.K., Trewin, B., Villarreal, C., Vincent, L.A., Zhai, P., Zhang, X., Kitching, S., 2013. Updated analyses of temperature and precipitation extreme indices since the beginning of the twentieth century: the HadEX2 dataset. *J. Geophys. Res., Atmos.* 118, 2098–2118.
- Dunkley Jones, T., Lunt, D.J., Schmidt, D.N., Ridgwell, A., Sluijs, A., Valdes, P.J., Maslin, M., 2013. Climate model and proxy data constraints on ocean warming across the Paleocene–Eocene Thermal Maximum. *Earth-Sci. Rev.* 125, 123–145.
- Emori, S., Brown, S.J., 2005. Dynamic and thermodynamic changes in mean and extreme precipitation under changed climate. *Geophys. Res. Lett.* 32, 1–5.

- Evans, J.P., Westra, S., 2012. Investigating the mechanisms of diurnal rainfall variability using a regional climate model. *J. Climate* 25, 7232–7247.
- Foreman, B.Z., Heller, P.L., Clementz, M.T., 2012. Fluvial response to abrupt global warming at the Palaeocene/Eocene boundary. *Nature* 490, 92–95.
- Gervais, M., Tremblay, L.B., Gyakum, J.R., Atallah, E., 2014. Representing extremes in a daily gridded precipitation analysis over the United States: impacts of station density, resolution, and gridding methods. *J. Climate* 27, 5201–5218.
- Gordon, C., Cooper, C., Senior, C.A., Banks, H., Gregory, J.M., Johns, T.C., Mitchell, J.F.B., Wood, R.A., 2000. The simulation of SST, sea ice extents and ocean heat transports in a version of the Hadley Centre coupled model without flux adjustments. *Clim. Dyn.* 16, 147–168.
- Handley, L., O'Halloran, A., Pearson, P.N., Hawkins, E., Nicholas, C.J., Schouten, S., McMillan, I.K., Pancost, R.D., 2012. Changes in the hydrological cycle in tropical East Africa during the Paleocene–Eocene Thermal Maximum. *Palaeogeogr. Palaeoclimatol. Palaeoecol.* 329, 10–21.
- Hartmann, D.L., Klein-Tank, A.M.G., Rusticucci, M., Alexander, L.V., Brönnimann, S., Charabi, Y., Dentener, F.J., Dlugokencky, E.J., Easterling, D.R., Kaplan, A., Soden, B.J., Thorne, P.W., Wild, M., Zhai, P.M., 2013. Observations: atmosphere and surface. In: Stocker, T.F., Qin, D., Plattner, G.-K., et al. (Eds.), *The Physical Science Basis. Contribution of Working Group I to the Fifth Assessment Report of the Intergovernmental Panel on Climate Change*. Cambridge University Press, Cambridge, United Kingdom, pp. 159–254.
- Huber, M., Caballero, R., 2011. The early Eocene equable climate problem revisited. *Clim. Past* 7 (2), 603–633.
- Huber, M., Goldner, A., 2012. Eocene monsoons. *J. Asian Earth Sci.* 44, 3–23.
- Hunter, S.J., Haywood, A.M., Valdes, P.J., Francis, J.E., Pound, M.J., 2013. Modelling equable climates of the Late Cretaceous: can new boundary conditions resolve data–model discrepancies? *Palaeogeogr. Palaeoclimatol. Palaeoecol.* 392, 41–51.
- John, C.M., Bohaty, S.M., Zachos, J.C., Sluijs, A., Gibbs, S., Brinkhuis, H., Bralower, T.J., 2008. North American continental margin records of the Paleocene–Eocene thermal maximum: implications for global carbon and hydrological cycling. *Palaeoceanography* 23.
- Kandel, D.D., Western, A.W., Grayson, R.B., Turrill, H.N., 2004. Process parameterization and temporal scaling in surface runoff and erosion modelling. *Hydrol. Process.* 18, 1423–1446.
- Kraus, M.J., McInerney, F.A., Wing, S.L., Secord, R., Baczynski, A.A., Bloch, J.L., 2013. Paleohydrologic response to continental warming during the Paleocene–Eocene Thermal Maximum, Bighorn Basin, Wyoming. *Palaeogeogr. Palaeoclimatol. Palaeoecol.* 370, 196–208.
- Kraus, M.J., Riggins, S., 2007. Transient drying during the Paleocene–Eocene Thermal Maximum (PETM): analysis of paleosols in the Bighorn Basin, Wyoming. *Palaeogeogr. Palaeoclimatol. Palaeoecol.* 245 (3–4), 444–461.
- Lenderink, G., van Meijgaard, E., 2008. Increase in hourly precipitation extremes beyond expectations from temperature changes. *Nat. Geosci.* 1, 511–514.
- Li, F., Rosa, D., Collins, W.D., Wehner, M.F., 2012. Super-parameterization: a better way to simulate regional extreme precipitation. *J. Adv. Model. Earth Syst.* 4, M04002.
- Loptson, C.A., Lunt, D.J., Francis, J.E., 2014. Investigating vegetation–climate feedbacks during the early Eocene. *Clim. Past* 10 (2), 419–436.
- Lunt, D.J., et al., 2017. The DeepMIP contribution to PMIP4: experimental design for model simulations of the EECO, PETM, and pre-PETM (version 1.0). *Geosci. Model Dev.* 10, 889–901.
- Lunt, D.J., Flecker, R., Valdes, P.J., Salzmann, U., Gladstone, R., Haywood, A.M., 2008. A methodology for targeting palaeo data acquisition: a case study for terrestrial late Miocene. *Earth Planet. Sci. Lett.* 271, 53–62.
- Lunt, D.J., Valdes, P.J., Jones, T.D., Ridgwell, A., Haywood, A.M., Schmidt, D.N., Marsh, R., Maslin, M., 2010. CO₂-driven ocean circulation changes as an amplifier of Paleocene–Eocene thermal maximum hydrate destabilization. *Geology* 38, 875–878.
- Nearing, M.A., Pruski, F.F., O'Neal, M.R., 2004. Expected climate change impacts on soil erosion rates: a review. *J. Soil Water Conserv.* 59, 43–50.
- O'Gorman, P.A., 2015. Precipitation extremes under climate change. *Curr. Clim. Change Rep.* 1, 49–59.
- Pagani, M., Pedentchouk, N., Huber, M., Sluijs, A., Schouten, S., Brinkhuis, H., Damsté, J.S.S., Dickens, G.R., 2006. Arctic hydrology during global warming at the Palaeocene/Eocene thermal maximum. *Nature* 442, 671–675.
- Pearson, P.N., Nicholas, C.J., Singano, J.M., Bown, P.R., Coxall, H.K., van Dongen, B.E., Roberts, A.P., 2004. Paleogene and Cretaceous sediment cores from the Kilwa and Lindi areas of coastal Tanzania: Tanzania Drilling Project Sites 1–5. *J. Afr. Earth Sci.* 39 (1–2), 25–62.
- Pierrehumbert, R.T., 2002. The hydrologic cycle in deep-time climate problems. *Nature* 419 (6903), 191–198.
- Pujalte, V., Baceta, J., Schmitz, B., 2015. A massive input of coarse-grained siliciclastics in the Pyrenean Basin during the PETM: the missing ingredient in a coeval abrupt change in hydrological regime. *Clim. Past* 11, 1653–1672.
- Sachse, D., Billaut, I., Bowen, G.J., Kahmen, A., 2012. Molecular paleohydrology: interpreting the hydrogen-isotopic composition of lipid biomarkers from photosynthesising organisms. *Annu. Rev. Earth Planet. Sci.* 40, 221–249.
- Schmitz, B., Pujalte, V., 2007. Abrupt increase in seasonal extreme precipitation at the Paleocene–Eocene boundary. *Geology* 35 (3), 215–218.
- Scoccimarro, E., Gualdi, S., Bellucci, A., Zampieri, M., Navarra, A., 2013. Heavy precipitation events in a warmer climate: results from CMIP5 models. *J. Climate* 26 (20), 7902–7911.
- Sluijs, A., Bijl, P.K., Schouten, S., Röhl, U., Reichert, G.J., Brinkhuis, H., Rohl, U., 2011. Southern ocean warming, sea level and hydrological change during the Paleocene–Eocene thermal maximum. *Clim. Past* 7 (1), 47–61.
- Sluijs, A., Van Roij, L., Harrington, G.J., Schouten, S., Sessa, J.A., Levay, L.J., Reichert, G.J., Slomp, C.P., 2014. Warming, euxinia and sea level rise during the Paleocene–Eocene thermal maximum on the gulf coastal plain: implications for ocean oxygenation and nutrient cycling. *Clim. Past* 10, 1421–1439.
- Smith, F., Wing, S., Freeman, K., 2007. Magnitude of the carbon isotope excursion at the Paleocene–Eocene thermal maximum: the role of plant community change. *Earth Planet. Sci. Lett.* 262, 50–65.
- Smith, J.J., Hasiotis, S.T., Woody, D.T., Kraus, M.J., 2008. Paleoclimatic implications of crayfish-mediated prismatic structures in paleosols of the Paleogene Willwood Formation, Bighorn Basin, Wyoming, U.S.A. *J. Sediment. Res.* 78, 323–334.
- Speelman, E.N., Sewall, J.O., Noone, D., Huber, M., von der Heydt, A., Damsté, J.S., Reichert, G.J., 2010. Modeling the influence of a reduced equator-to-pole sea surface temperature gradient on the distribution of water isotopes in the Early/Middle Eocene. *Earth Planet. Sci. Lett.* 298 (1–2), 57–65.
- Sun, Y., Solomon, S., Dai, A., Portmann, R.W., 2006. How often does it rain? *J. Climate* 19, 916–934.
- Trenberth, K.E., 2011. Changes in precipitation with climate change. *Clim. Res.* 47, 123–138.
- Turner, A.G., Slingo, J.M., 2009. Uncertainties in future projections of extreme precipitation in the Indian monsoon region. *Atmos. Sci. Lett.* 10, 152–158.
- Valdes, P.J., Armstrong, E., Badger, M.P.S., Bradshaw, C.D., Bragg, F., Davies-Barnard, T., Day, J.J., Farnsworth, A., Hopcroft, P.O., Kennedy, A.T., Lord, N.S., Lunt, D.J., Marzocchi, A., Parry, L.M., Roberts, W.H.G., Stone, E.J., Tourte, G.J.L., Williams, J.H.T., 2017. The BRIDGE HadCM3 family of climate models: HadCM3@Bristol v1.0. *Geosci. Model Dev.* 10, 3715–3743.
- Willison, J., Robinson, W.A., Lackmann, G.M., 2015. North Atlantic storm-track sensitivity to warming increases with model resolution. *J. Climate* 28, 4513–4524.
- Wing, S.L., Harrington, G.J., Smith, F.A., Bloch, J.L., Boyer, D.M., Freeman, K.H., 2005. Transient floral change and rapid global warming at the Paleocene–Eocene boundary. *Science* 310, 993–996.
- Zhang, X., Alexander, L., Hegerl, G.C., Jones, P., Tank, A.K., Peterson, T.C., Trewin, B., Zwiers, F.W., 2011. Indices for monitoring changes in extremes based on daily temperature and precipitation data. *Wiley Interdiscip. Rev.: Clim. Change* 2, 851–870.